 doi:10.20944/preprints202106.0078.v1



# Discrete element modelling of pit crater formation on Mars

**Stuart Hardy**[1,2]

1. ICREA (Institució Catalana de Recerca i Estudis Avançats), Passeig Lluís Companys 23. 08010 Barcelona, Catalonia, Spain.
2. Facultat de Geologia, Universitat de Barcelona, 08028 Barcelona, Catalonia, Spain.
email: stuart.hardy@icrea.cat tel:+34 934 02 13 76

**Abstract**

Pit craters, and pit crater chains, are now recognised as being an important part of the surface morphology and structure of many planetary bodies, and are particularly remarkable on Mars. Pit craters do not possess the elevated rims, ejecta deposits, or other features that are typically associated with *impact* craters. They are thought to arise from the drainage/collapse of a *relatively* weak surficial material into an open (or widening) void in a much stronger material below. The creation of such voids has been suggested to be due to extensional fracturing/dilational faulting, shallow dike intrusion, lava tube collapse amongst other hypotheses. These craters have a very distinctive expression, often presenting funnel, cone, or bowl-shaped geometries. Analogue models of pit crater formation provide a map-view picture of their initiation and evolution but give little insight into their internal structure or geometry, but produce pits that typically have steep, nearly conical cross sections. Numerical modelling studies of their formation have been limited and have produced some quite interesting, but nonetheless puzzling, results whereby the simulated pit craters had generally convex (steepening downward) slope profiles with no distinct rim; quite unlike many of those observed on Earth or on Mars. To address these issues, I present here a high-resolution, 2D discrete element model of weak cover (regolith) collapse into either a static or a widening underlying void. I use frictional and frictional-cohesive discrete elements to represent a range of probable cover rheologies. Under Martian gravitational conditions, frictional-cohesive and frictional materials produce cone, bowl and scoop-shaped pit craters. For a given cover thickness, the specific crater shape depends on the amount of underlying void space created for drainage. When void space is small relative to cover thickness, craters have bowl or scoop-shaped geometries. In contrast, when void space is large relative to cover thickness, craters have cone-shaped geometries with essentially planar (nearing angle of repose) slope profiles. Frictional-cohesive materials exhibit more distinct rims than simple frictional materials and thus may reveal some stratigraphic layering on the pit crater walls. In the limit, when drainage from the overlying cover is insufficient to fill the underlying void, ´skylights´ into the deeper structure are created. Implications of these results for the interpretation of pit craters on Earth, Mars, other planets and moons are discussed.

## Introduction

Pit craters and pit crater chains are now recognised as being an important part of the surficial morphology and structure of many planetary bodies (e.g., Horstman and Melosh, 1989; Sims *et al*., 2003; Wyrick *et al*., 2004; Smart *et al*, 2011; Cushing, 2012; Michikami *et al*., 2014; Martin *et al*., 2017; Fig. 1a,b). They have a very distinctive expression, often presenting funnel, cone, or bowl-shaped geometries, and do not possess the elevated rim, ejecta deposits, or other features that are typically associated with *impact* craters. (Fig. 1a,b). They are depressions that typically have circular-elliptical plan view shapes, and, in some cases, flat floors. Exceptionally, they may provide ´skylights´ into the underlying void (Cushing, 2012; Fig. 1b). They do not appear to modify the planetary surface beyond their edges. They are thought to arise from the drainage and/or collapse of weak surficial material into an open void in stronger material below. The origin of such craters is somewhat contentious (see Smart *et al*., 2011; Ferrill *et al*., 2011; Martin *et al*., 2017). However, their morphology and geometric relations have led many authors to conclude that they are the surface traces of open voids or fractures in an underlying solid body — perhaps due to extensional fracturing/dilational faulting, shallow dike intrusion or lava tube collapse, amongst other hypotheses. Analogue models of pit crater formation provide a map-view picture of their initiation and evolution but give little insight into the internal structure of such craters (e.g., Horstman and Melosh, 1989; Sims *et al*., 2003; Ferrill *et al*., 2004). Horstman and Melosh (1989) described their analogue pit craters as being "a cone-shaped region with apex at the bottom the regolith and with a slope angle of about 30°" equivalent to measured angles of repose for their regolith material, whilst those of Sims *et al*. (2004) are visibly and clearly cone-shaped with steep walls. Numerical modelling studies of their formation have been limited and have produced some quite interesting, but puzzling, results whereby the simulated pits in both weak, frictional and "strong" materials had generally convex (steepening downward) slope profiles with no

Preprints (www.preprints.org) | NOT PEER-REVIEWED | Posted: 2 June 2021 doi:10.20944/preprints202106.0078.v1



distinct rim, and where angle of repose slopes were not produced; quite unlike those observed on Earth, Mars or in analogue modelling studies (Smart *et al*., 2011; Fig. 1c). In contrast, conceptual models of pit crater drainage do not show these features, typically they depict a cone-shaped craters with a distinct rim, and with angle of repose wall slopes that are planar and not downward steepening at all (Fig. 1d). In addition, some Mars Orbiter images seem to show a kind of stratification in pit crater walls, and this may indicate that, rather than being simply unconsolidated, granular materials, the cover (regolith) may well possess *some* cohesive strength; this hypothesis is reinforced by the occurrence of distinct, sharp rims in many pit craters and fault scarps, graben and other features in regolith at the planetary surface. Here, I present a high-resolution (1-2 m) discrete element model of cover collapse above either a simple static or a widening underlying void (Fig. 1e,f). I use frictional and frictional-cohesive discrete elements to represent a range of probable cover rheologies. Under Martian gravitational conditions, these materials produce cone, scoop and bowl-shaped pit craters. For a given regolith thickness, the specific pit crater geometry depends on the amount of underlying space created. No significant difference is seen between craters produced above static versus widening voids. When void space is small relative to cover thickness, craters have bowl or scoop-shaped geometries. In contrast, when void space is large relative to cover thickness, crater walls have essentially planar (approaching angle of repose) slope profiles. Frictional-cohesive materials develop craters with more distinct rims and may reveal some stratigraphic layering on pit crater walls. In the limit, when regolith thickness is insufficient to fill the underlying void, ´skylights´ into the deeper structure are created. Implications of these results for the interpretation of pit craters on Earth, Mars, other planets and moons are discussed.

**Methodology**

Here I use a 2D discrete element numerical model to simulate the growth of (collapse) pit craters in a weak cover/regolith above an underlying void in strong basement. Modelling of deformation to high strain is an ideal candidate for the discrete element technique as it is well-suited to studying problems in which discontinuities (shear-zones, faults, fractures, voids etc) are important. It also allows deformation involving unlimited relative motions of individual elements and complex, abrupt and changing boundary conditions (Cundall & Strack, 1979; Finch *et al*., 2004: Egholm *et al*., 2007; Hardy, 2008, 2011, 2019a; Thompson *et al*., 2010), particularly germane to the simulation/formation of pit craters. The discrete element code used here to undertake these simulations is ¨cdem2D¨ which has been used previously to undertake a wide variety of structural geology modelling in both 2D and 3D (as cdem3D). The basic numerical methodology and its application to a variety of problems (fault-propagation folding, orogenic wedge growth, caldera collapse, dike intrusion on Mars, viscous flow, Gilbert deltas, etc.) have been published previously (e.g., Botter *et al.,* 2014, 2016; Hardy, 2008; Hardy *et al.,* 2009; Hardy, 2016; Hardy, 2018; Hardy, 2019a,b). Of particular interest here, the details of this code applied to frictional and frictional-cohesive materials can be found elsewhere (e.g., Hardy *et al*., 2009; Hardy 2011, 2015, 2019b). Here, I will illustrate the use of this modelling scheme to simulate the growth of pit craters on Mars.

**Model parameters, set-up and boundary conditions**

Below I present the results of two sets of simple, end-member numerical models (experiments) of pit crater formation. In each case, I will examine the collapse/drainage of a (relatively) weak regolith material into a void at the regolith/basement interface (Fig. 1e,f). The regolith has a uniform thicknesses of 100 m and all models are 400 m wide. The void into which collapse occurs grows either as a result of the incremental widening of a dilational, extension fracture (Series 1 Experiments; Fig. 1e), or is created instantaneously, simulating roof collapse into e.g. a lava tube (Series 2 Experiments; Fig. 1f). In both experimental series, two different void geometries are considered in order to examine pit craters created where the amount of void space relative to regolith thickness is small and large respectively. The voids created have 2 distinct areas: 100 x 40 and 300 x 40 m, allowing for the regolith to experience limited and significant drainage respectively. Obviously, the voids that are created do not represent the *actual geometry* of any individual void space but, rather, create space for *potential drainage* of the regolith. The model represents the regolith section (the cover above the basement) and the walls/faults using approximately 19,000 discrete elements. Element radii range from 0.5 to 1.25 m (average radius 0.77 m) and their density is 2000 kg/m$^3$. The regolith is coloured using 12 red and yellow layers to highlight deformation but these layers have no mechanical significance (Fig. 1e,f).

The discrete elements making up the cover obey Newton's equations of motion and interact with each other under the influence of Martian gravity. Elements experience Mohr-Coulomb frictional contact interactions with their neighbours (see Finch *et al*., 2004 and Hardy *et al*., 2009 for a full description of the

Preprints (www.preprints.org) | NOT PEER-REVIEWED | Posted: 2 June 2021 doi:10.20944/preprints202106.0078.v1



modelling approach). In discrete element models such as that used here parameters such as the strength, coefficient of friction etc, of an assemblage are emergent properties and do not relate directly to micro-properties. They are typically assessed through the use of angle of repose and/or unconfined/confined biaxial numerical tests (cf. Oger *et al*., 1998; Finch *et al*., 2004; Holohan *et al*., 2011; Botter *et al*., 2014; Hardy, 2019a). Using such tests, the frictional-cohesive discrete elements used here have been found to have a bulk coefficient of friction (μ) of c. 0.70 (internal angle of friction (ø) of c. 35°) and (where present) to have a cohesion of c. 0.1 MPa. These friction and cohesion values lie within the ranges reported for natural sedimentary, granular materials and are much smaller than those typically derived from centimetre-scale laboratory samples of strong, lithified rocks (cf. Schultz, 1996; Strayer *et al*., 2004; Holohan *et al*., 2011), but do lie within the ranges reported for natural unconsolidated or weakly consolidated rock masses (cf. Schultz, 1996; Strayer *et al*., 2004; Holohan *et al.,* 2011).

Here I examine the effect of the creation of a 40 m wide vertical void in rigid basement on regolith drainage and pit crater formation; this void either grows incrementally until it reaches its final width or appears instantaneously as a result of collapse over the roof width (Fig. 1e,f). In the case of incremental void growth, this is modelled by using two rigid basement walls placed edge to edge. Dilational growth of the fracture is simulated by slowly drawing the walls 40 m apart over the first 10% of the model run, and allowing concurrent drainage of regolith into the evolving void; after the final width is achieved, simple drainage into a static void occurs. In the case of instantaneous roof collapse, the walls are placed 40 m apart at the start of the model run, the void "roof" is removed and drainage occurs immediately. Models are run for a total model simulated time of 36,000 seconds, sufficient to ensure that all elements reach a static equilibrium, and the final configuration of the simulation is achieved.

As the experiments proceed, the effect of the drainage of regolith elements into the underlying void is transmitted upwards into the cover, changing local element interactions and thus contact forces. As a result of this change in local forces, the internal elements are advanced to their new positions within the model by integrating their equations of motion using Newtonian physics and a velocity-Verlet based numerical scheme (cf. Mora and Place, 1993). Element positions are saved during experiments to allow a detailed, high-resolution analysis of geometry, displacement and strain (cf. Cardozo & Allmendinger, 2009). The numerical code used (cdem2D) has been parallelised using OpenMP and has been thoroughly tested and verified against the serial version (cf. Chapman *et al*., 2007; Hardy, 2015). Typical experiments like those discussed here take ~12 hours to run on a desktop machine with two 6-core Intel Xeon (X5650 - 2.66 GHz) processors allowing 24 computational threads. Model results are saved at regular intervals throughout as ¨time snapshots¨.

For each experiment discussed herein many different models have been run with parameters similar to those described above. However, the specific experiments discussed are representative of the evolution typically observed under these boundary conditions in that they contain the reproducible, characteristic features seen in many models. The important scientific message to be taken away is not the precise location of an individual geometric feature, but rather the distinctive, reproducible, behaviours that emerge from multiple experiments.

**Series 1 Experiments - Progressively Opening Void (Extension Fracture)**

In the first series of experiments (Figure 2), I will show the effect of a progressively opening void (extension fracture) on an overlying regolith with either a simple frictional or a frictional-cohesive rheology. As discussed above, two distinct types of void will be considered — one of which has a small (potential) drainage area relative to the regolith thickness and another which has a larger (potential) drainage area. In each case, I will examine/describe the resultant geometries and their characteristic features at the end of the model run, when all elements are static.

*Small relative drainage area* - Shown in Figure 2a is the final geometry as a result of collapse of the simple frictional regolith into the smaller void and, in Fig. 2b, that of the frictional-cohesive regolith. In both cases, we see that the small relative drainage area leads to bowl-scoop shaped crater geometries, sometimes exhibiting an almost flat base. In no cases are angle of repose (c. 35°) slopes produced, but also note that the slopes of the crater walls do not *steepen* downwards, in fact they flatten to a sub-horizontal central area from approximately 25 degrees at the crater edges. The crater rim is less well defined in the purely frictional (granular) regolith (Fig. 2a), and is very marked in the frictional-cohesive regolith (Fig. 2b). Clearly, if the crater rim is ill-defined then some appearance of steepening downward profiles in this region can be produced, but no systematic downward steepening of crater walls is observed. In addition, with frictional-cohesive regolith we see a rougher upper crater surface due to the formation of a number of small fault

 doi:10.20944/preprints202106.0078.v1



scarps. The maximum heights of these scarps are around 10 m consistent with a low, but finite, cohesive strength. The maximum depths of the craters are of the order of approximately 30 m (compared to an initial regolith thickness of 100 m) and they have widths of approximately 150-170 m.

*Large relative drainage area* - Shown in Figure 2c is the final geometry as a result of collapse of the simple frictional regolith into the larger void and, in Fig. 2d, that of the frictional-cohesive regolith. In both cases, we see that a larger relative drainage area leads to very distinctive, cone-shaped, geometries, with almost planar crater walls dipping at around 33-35 degrees. Such geometries are very different to those produced above the smaller void (compare Fig. 2a,b and Fig. 2c,d). The simple, frictional regolith produces quite smooth crater walls, whilst in the case of the frictional-cohesive regolith, we see a rougher upper crater surface due to small fault scarps, cliffs and open fissures. Maximum scarp or cliff heights are around 10 m consistent with the finite, but low, cohesive strength of the regolith material. In both cases, the crater walls meet at a singular point centrally located above the infilled void. In addition, in the upper parts of the crater walls one can see part of the "stratigraphy" of the regolith exposed, whereas other parts of the craters walls are "mantled" by drained-collapsed material lacking internal structure. The maximum depths of the craters are similar in both cases and are of the order of around 85-90 m (compared to an initial regolith thickness of 100 m) and they have widths of approximately 230-250 m.

**Series 2 Experiments - Instantaneous Roof Collapse**

In the second series of experiments (Figure 3), I will show the effect of a void which instantaneously appears as a result of "roof" collapse and allows drainage of an overlying regolith with either a simple frictional or a frictional-cohesive rheology. As before, two distinct voids will be considered — one of which has a small (potential) drainage area relative to the regolith thickness, and another which has a larger (potential) area for drainage. In each case, I will examine/describe the resultant geometries and their characteristic features at the end of the model run, when all elements are static.

*Small relative drainage area* - Shown in Figure 3a is the result of collapse of the simple frictional regolith into the smaller void and, in Fig. 3b, that of the frictional-cohesive regolith. In both cases, as with the progressively widening void, we see that a small relative void area leads to bowl-scoop shaped geometries, with an almost flat base. In no cases are angle of repose crater wall slopes produced, in addition the slopes of the crater walls do not *steepen* downward. The crater rim is less well-defined in the purely frictional (granular) regolith (Fig. 3a), while it is very marked in the frictional-cohesive regolith (Fig. 3b). In the case of the frictional-cohesive cover we see a more stepped, rougher upper surface due to a number of small fault scarps, cliffs and fissures, maximum scarp heights are around 10 m consistent with the low cohesive strength of the regolith. The maximum depths of the pit craters are of the order of approximately 25-30 m (compared to an initial regolith thickness of 100 m) and they have widths of approximately 135-150 m.

*Large relative drainage area* - Shown in Figure 3c is the result of collapse of the simple frictional regolith into the larger void and, in Fig. 3d, that of the frictional-cohesive regolith. In both cases, as with the progressively widening void, we see that a large relative void area leads to cone-shaped geometries, with almost planar sidewalls dipping at around 30-35 degrees (approaching angle of repose). In the case of the frictional-cohesive regolith, we see a rougher upper surface due to small faults, cliffs, open fissures and overhangs consistent with the low cohesive strength of the regolith. Such craters meet at a singular point centrally located above the infilled void. This allows us to see some stratigraphy in the upper parts of the pit craters. The maximum depths of the craters are of the order of around 85-90 m (compared to an initial regolith thickness of 100 m) and they have widths of approximately 220-230 m.

**Discussion and Conclusions**

In this short paper I have simulated, using the discrete element method, the drainage of a (*relatively*) weak cover (regolith) material into an underlying void in stronger basement, and the consequent creation of pit craters. Many of the distinctive features of pit craters seen on Mars have been reproduced, including bowl-scoop shaped geometries, cone-shaped geometries, district crater rims and angle of repose wall slopes. Whether the underlying void opens progressively (as an extension fracture) or appears instantaneously (as a result of roof collapse) makes little difference to the final surficial expression of the pit crater. What makes a significant difference, however, is the relative area of the void created compared to the thickness of the regolith. When void space is small relative to cover thickness, craters have bowl or scoop-shaped geometries. In contrast, when void space is large relative to cover thickness, craters have more cone-shaped geometries

Preprints (www.preprints.org) | NOT PEER-REVIEWED | Posted: 2 June 2021 doi:10.20944/preprints202106.0078.v1



with essentially planar (approaching the angle of repose) slope profiles. In every case, frictional-cohesive regolith materials exhibit more distinct rims than simple frictional materials and thus may reveal some stratigraphic layering (if present) in the upper pit crater walls.

Several key observations arise from these simulations. Firstly, this study emphasises that pit crater walls can exhibit both angle of repose slopes (c. 35° in this case e.g. Fig 2d) and stable, more gentle collapse slopes (c. 20° or less, Fig. 3a,b). Angle of repose wall slopes tend to occur when there has been significant drainage into the underlying void. Secondly, the simulations also highlight that pit crater depth only provides a *minimum* estimate of regolith thickness as there is no *a priori* reason to assume that void area (in 2D) should always be sufficient to drain to the regolith-basement contact. Previous studies have applied geometric relationships based on cone shapes and angle of repose slopes to estimate pit depth and volume (e.g., Wyrick *et al*., 2004; Martin and Whitten, 2018). In general, this study shows that only cone-shaped pits give a reasonable estimate (proxy) of regolith thickness, whereas bowl or scoop-shaped pits provide, at best, a minimum estimate. Thirdly, it appears that craters with distinct, sharp, rims like those seen on Mars are only formed when the regolith has *some* cohesive strength. Such a weakly cohesive regolith also produces open fissures, cliffs, faults and exposes regolith "stratigraphy" in the uppermost part of the crater walls (Fig. 2b,d; Fig. 3b,d; Fig. 4a) whilst lower parts of craters walls are mantled by disrupted, collapsed materials (Fig. 4b). This is consistent with the occurrence of fault scarps and graben systems in Martian regolith (Ferrill *et al*., 2011), and suggests that in order to simulate, and understand, Martian pit craters a frictional-cohesive cover or regolith is necessary. Finally, this study has shown that bowl, scoop, cone and funnel-shaped crater geometries can all exist, and that they represent a spectrum of potential geometries.

Obviously, in the limit, it is entirely possible that drainage from the overlying regolith may be insufficient to fill any underlying void (either the void is too large or the regolith is too thin). In such a situation, it has been suggested that ´skylights´ into the underlying void can be created (Cushing, 2012). These have been proposed as candidate cave entrances into Martian near-surface lava tubes and volcano-tectonic fracture systems. Such Martian caves have even been suggested as "promising potential sites for future human habitation and astrobiology investigations" (Cushing, 2012). Using the same experimental set-up as the Series 2 experiments, I show here what happens if this were to be the case for a frictional-cohesive regolith (Fig. 4c). The experiment presented here is a roof collapse model, identical to the other examples, but with a very "deep" void (500 m) into which to drain the regolith, thus there is more "volume" than available regolith material. This simulation is run for 3 times as long as the other experiments in order to reach a static equilibrium. From the final result we see that, indeed, a ´skylight´ into the underlying void is created under these conditions; with steep crater walls terminating at the regolith-basement interface and a partially filled "void" below (Fig. 4c).

However, the question does arise as to why the results of these numerical simulations are so different to those presented by Smart *et al*. (2011). They investigated a very similar scenario to that presented here: an extension fracture underlying either a weak, unconsolidated regolith or a regolith containing strong "rock" layers (Fig. 1c). They also examined a dilational fault underlying a regolith, which is not considered herein. For purely frictional, granular, ´weak´ materials, they produced some quite interesting, but nonetheless puzzling, results whereby the simulated pit craters had generally *convex* (steepening downward) slope profiles and no distinct rim; quite unlike many of those observed on Earth or on Mars (Fig. 1c). Without knowing the bulk coefficient of friction of their unconsolidated material (no calibrated angle of friction was quoted) or the bulk density of the regolith, it is difficult to speculate on the origin of these differences. In order to address the idea that the Mars regolith might have *some* cohesive strength, they also simulated a cover which possessed a kind of mechanical stratigraphy. They did this by using several combinations of bonded elastic materials to represent moderate to very strong rock layers (cohesion ~7 MPa, unconfined compressive strength ~22 MPa), quite unlike those suggested for Martian regolith materials. These simulations still failed to reproduce the characteristic geometries of simple Martian pit craters, apart from producing highly fractured, block-like upper crater surfaces (Fig. 1c). In no case was any stratigraphic layering exposed in the crater walls. One notable difference is that the regolith used by Smart *et al*. was very thick (1000 m, compared to the 100 m thick regolith used here), but this scale difference should not affect the final crater geometries in frictional-cohesive materials. To illustrate this point, I show a final example of a roof collapse model beneath a 1000 m thick regolith which was run using the roof collapse experimental set-up presented herein (Fig. 4d). One clearly sees that the typical crater geometries seen in the 100 m thick regolith are produced as before (compare Fig. 3c and 4d).

Clearly, this paper is only an initial step in understanding the formation of pit craters on Mars and other planetary bodies and their moons. It is by no means complete, however the regolith rheologies examined so far have been simple but instructive and reproduce many key features observed on Mars. I have

also not examined here dilational faulting, where the void is produced as a result of a fault with a distinct throw. Finally, this study has been undertaken in 2D and the manner in which isolated pit craters grow and their spacing, form pit crater chains and spacing and their coalescence in 3D to form cuspate grooves and troughs, is of great interest. These, and other topics, are the focus of current research.

**Acknowledgements**

Discussions with, and the patience of, many colleagues over many years is appreciated; thanks must go particularly to Dave Waltham for stimulating my interest in numerical modelling and heavenly bodies many years ago. The author acknowledges the use of Mars Orbiter Camera images processed by Malin Space Science Systems that are available at http://www.msss.com/moc_gallery/. Discrete element modelling was carried out using cdem2D by the author.

**References**

Botter,C., Cardozo,N., Hardy,S., Lecomte,I. and Escalona,A. 2014. From mechanical modeling to seismic imaging of faults: A synthetic workflow to study the impact of faults on seismic. Marine and Petroleum Geology, 57, 187-207.

Botter,C., Cardozo,N., Hardy,S., Lecomte,I., Paton,G. and Escalona,A. 2016. Seismic characterisation of fault damage in 3D using mechanical and seismic modelling. Marine and Petroleum Geology, 77, 973-990.

Cardozo,N., and Allmendinger,R.W. 2009. SSPX: A program to compute strain from displacement/velocity data: Computers & Geosciences, 35, 1343-1357.

Chapman,B., Jost,G. and van der Pas,R. 2007. Using OpenMP : portable shared memory parallel programming. The MIT Press.

Cundall,P.A., and Strack,O.D.L. 1979. A discrete numerical model for granular assemblies: Geotechnique, 29, 47–65.

Cushing, G.E., 2012. Candidate cave entrances on Mars. J. Cave Karst Stud. 74, 33–47.

Egholm D.L., Sandiford M., Clausen O.R., and Nielsen S.B. 2007. A new strategy for discrete element numerical models: 2. Sandbox applications, Journal of Geophysical Research v. 112, B05204, doi: 10.1029/2006JB004558.

Ferrill,D.A., Wyrick, D.Y., and Smart,K.J. 2011. Coseismic, dilational-fault and extension-fracture related pit chain formation in Iceland: Analog for pit chains on Mars, Lithosphere 3(2):133-142
DOI: 10.1130/L123.1

Finch, E., Hardy, S., Gawthorpe, R.L., 2004. Discrete-element modelling of extensional fault-propagation folding above rigid basement fault blocks. Basin Research 16, 467–488.

Hardy,S. 2018. Coupling a frictional-cohesive cover and a viscous substrate in a discrete element model: First results of application to thick- and thin-skinned extensional tectonics, Marine and Petroleum Geology, 97, 32-44, ISSN 0264-8172, https://doi.org/10.1016/j.marpetgeo.2018.06.026.

Hardy S. 2019a.Discrete element modelling of extensional, growth, fault-propagation folds. Basin Res. 2019;31:584–599. https://doi. org/10.1111/bre.12335

Hardy, S. 2019b. Novel discrete element modelling of Gilbert-type delta formation in an active tectonic setting—first results. Basin Res. 2019; 31: 77–91. https://doi.org/10.1111/bre.12309

Holohan,E.P., Schopfer, M.P.J., and Walsh,J.J. 2011. Mechanical and geometric controls on the structural evolution of pit crater and caldera subsidence. Journal of Geophysical Research, 116, B07202, doi:1029/2010JB008032.

Horstman, K. C., and H. J. Melosh 1989. Drainage pits in cohesionless materials: Implications for the surface of Phobos, J. Geophys. Res., 94(B9), 12433–12441, doi: 10.1029/JB094iB09p12433.

E. S. Martin and J. L. Whitten 2018. Using Icelandic Pit Chains to Constrain Regolith Thickness on Saturn's Moon Enceladus. 49th Lunar and Planetary Science Conference 2018 (LPI Contrib. No. 2083)

Martin,E.S., Kattenhorn,S., Collins,G.C., Michaud,R.L Pappalardo,R.T. and Wyrick,D.Y. 2017. Pit Chains on Enceladus Signal the Recent Tectonic Dissection of the Ancient Cratered Terrains. Icarus, 294, 209-217.

T. Michikami, A. Hagermann, H. Miyamoto, S. Miura, J. Haruyama, P.S. Lykawka, 2014.
Impact cratering experiments in brittle targets with variable thickness: Implications for deep pit craters on Mars, Planetary and Space Science, 96, 71-80,https://doi.org/10.1016/j.pss.2014.03.010.

Mora,P., and Place,D. 1993. A lattice solid model for the non-linear dynamics of earthquakes: International Journal of Modern Physics C., 4, 1059–1074.

Oger, L., Savage,S.B., Corriveau, D., and Sayed,M. 1998. Yield and deformation of an assembly of disks subject to a deviatoric stress loading. Mechanics of Materials, 27, 189-210.
Sims, D.W., Morris, A.P., Ferrill, D.A., Wyrick, D.Y., and Colton, S.L. 2003. Physical Models of Pit Chain Formation over Dilational Faults on Mars: Lunar and Planetary Science Conference 34, Lunar and Planetary Institute, no. 2099.
Smart, K. J., D. Y. Wyrick, and D. A. Ferrill 2011. Discrete element modeling of Martian pit crater formation in response to extensional fracturing and dilational normal faulting, J. Geophys. Res., 116, E04005, doi:10.1029/2010JE003742.
Smart,K.J. & Ferrill,D.A. 2018, Discrete element modeling of extensional fault-related monocline formation. Journal of Structural Geology, 115, 82-90. https://doi.org/10.1016/j.jsg.2018.07.009
Thompson, N., Bennett, M.R., and Petford,N. 2010. Development of characteristic volcanic debris avalanche deposit structures: New insights from distinct element simulations. Journal of Volcanology and Geothermal Research, 192, 191-200.
Wyrick, D., D. A. Ferrill, A. P. Morris, S. L. Colton, and D. W. Sims 2004. Distribution, morphology, and origins of Martian pit crater chains, J. Geophys. Res., 109, E06005, doi:10.1029/2004JE002240.

**Figure Captions**

Preprints (www.preprints.org) | NOT PEER-REVIEWED | Posted: 2 June 2021 doi:10.20944/preprints202106.0078.v1



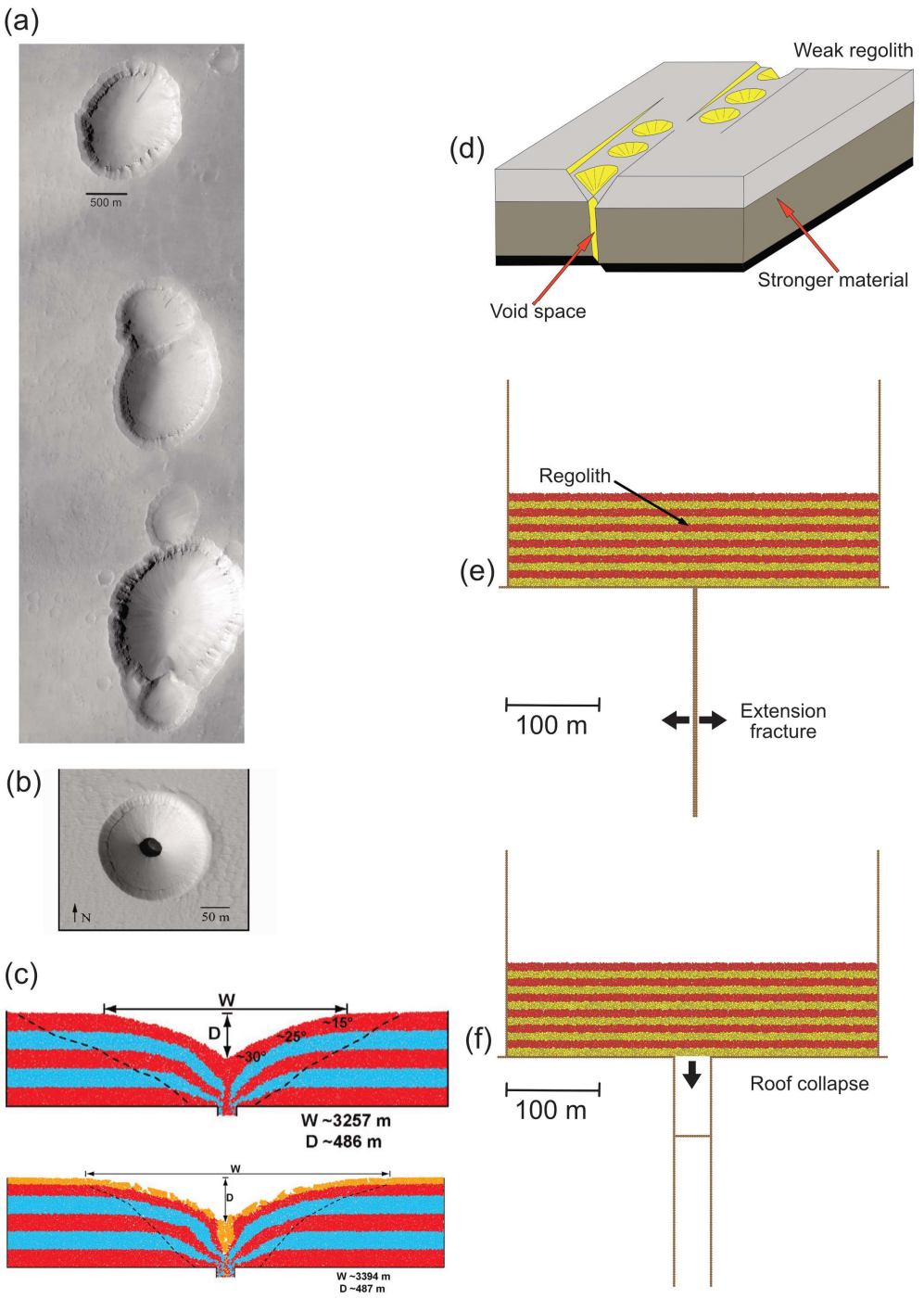


Figure 1

Figure 1. (a) Mars Orbiter image of part of a typical pit crater chain south of Alba Patera, Mars. MOC narrow angle image E0300254 courtesy of Malin Space Science Systems. Image location ~30.7°N, 113.7°W and (b) an example of a ′skylight′ pit crater from HiRISE image ESP_023531_1840 (3.71N, 248.51E) courtesy of NASA/JPL/University of Arizona, (c) top: example of a discrete element model of collapse pit formation in a frictional regolith above an extension fracture; bottom: in a frictional regolith with upper strong rock layer (orange), redrawn from Smart *et al*. 2011, (d) schematic diagram illustrating conceptual model of collapse pit formation above normal, dilational faults, redrawn from Ferrill *et al.* 2004, (e, f) boundary conditions and 2D model set-ups used in the experiments presented herein.

Preprints (www.preprints.org) | NOT PEER-REVIEWED | Posted: 2 June 2021 doi:10.20944/preprints202106.0078.v1



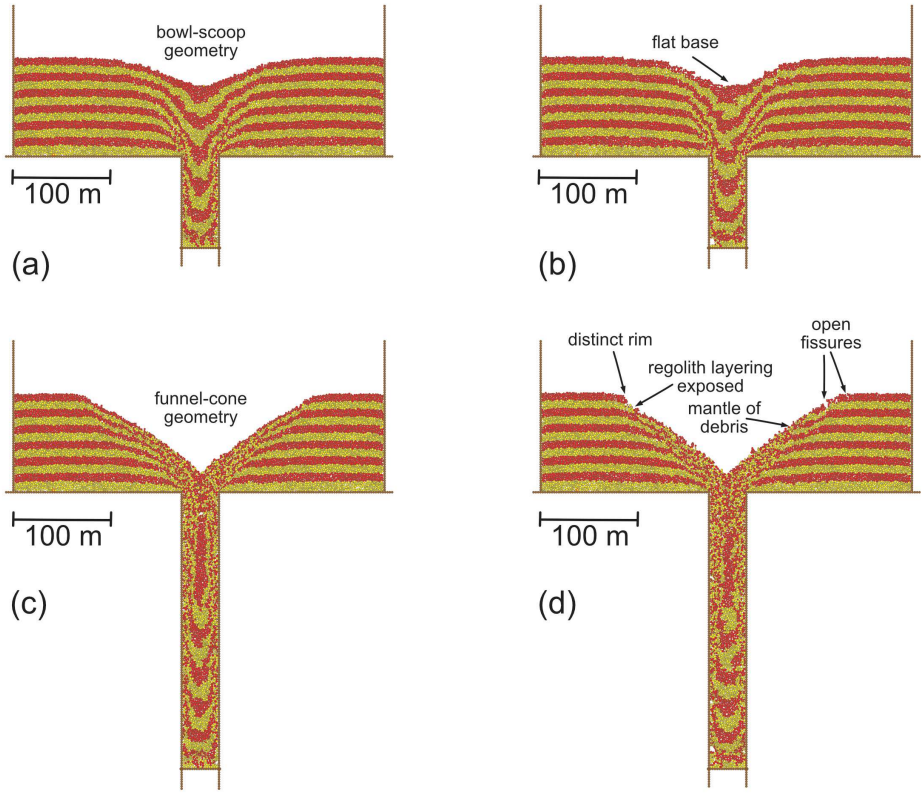


Figure 2

Figure 2. Series 1 experiments, final static configurations after progressive opening of a 40 m wide void. Void is either (a ,b) 100 m or (c, d) 300 m deep; in the left column the regolith is purely frictional, in the right column the regolith is frictional-cohesive, see text for discussion.

Preprints (www.preprints.org) | NOT PEER-REVIEWED | Posted: 2 June 2021 doi:10.20944/preprints202106.0078.v1



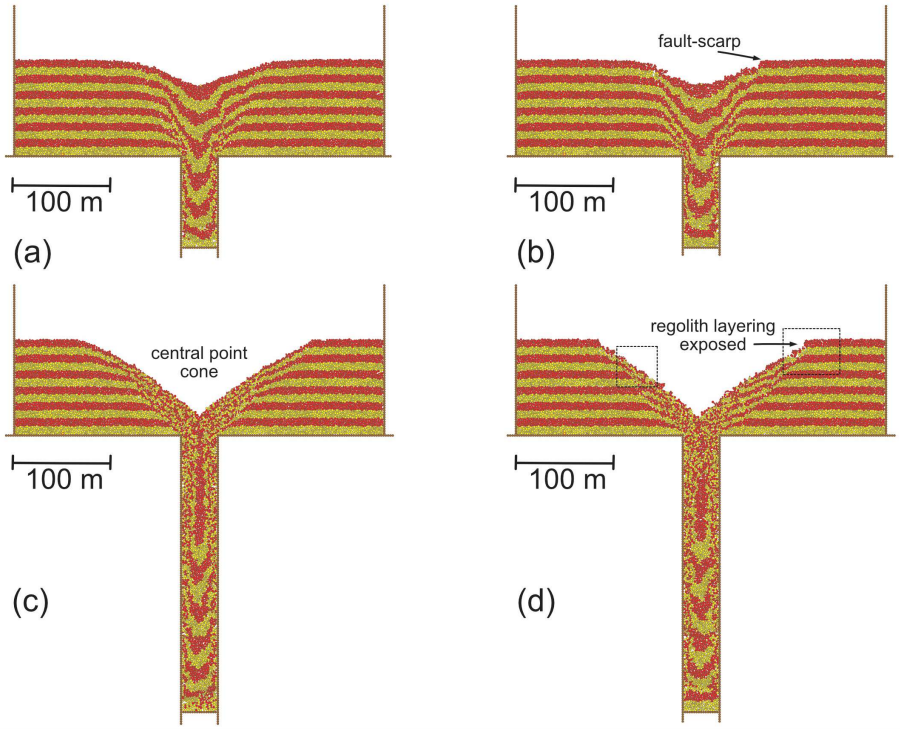


Figure 3

Figure 3. Series 2 experiments, final static configurations after instantaneous creation of a 40 m wide void. Void is either (a, b) 100 m or (c, d) 300 m deep; in the left column the regolith is purely frictional, in the right column the regolith is frictional-cohesive, see text for discussion. Dashed boxes in Fig. 3d indicate locations of "zooms" shown in Figure 4.

Preprints (www.preprints.org) | NOT PEER-REVIEWED | Posted: 2 June 2021 doi:10.20944/preprints202106.0078.v1



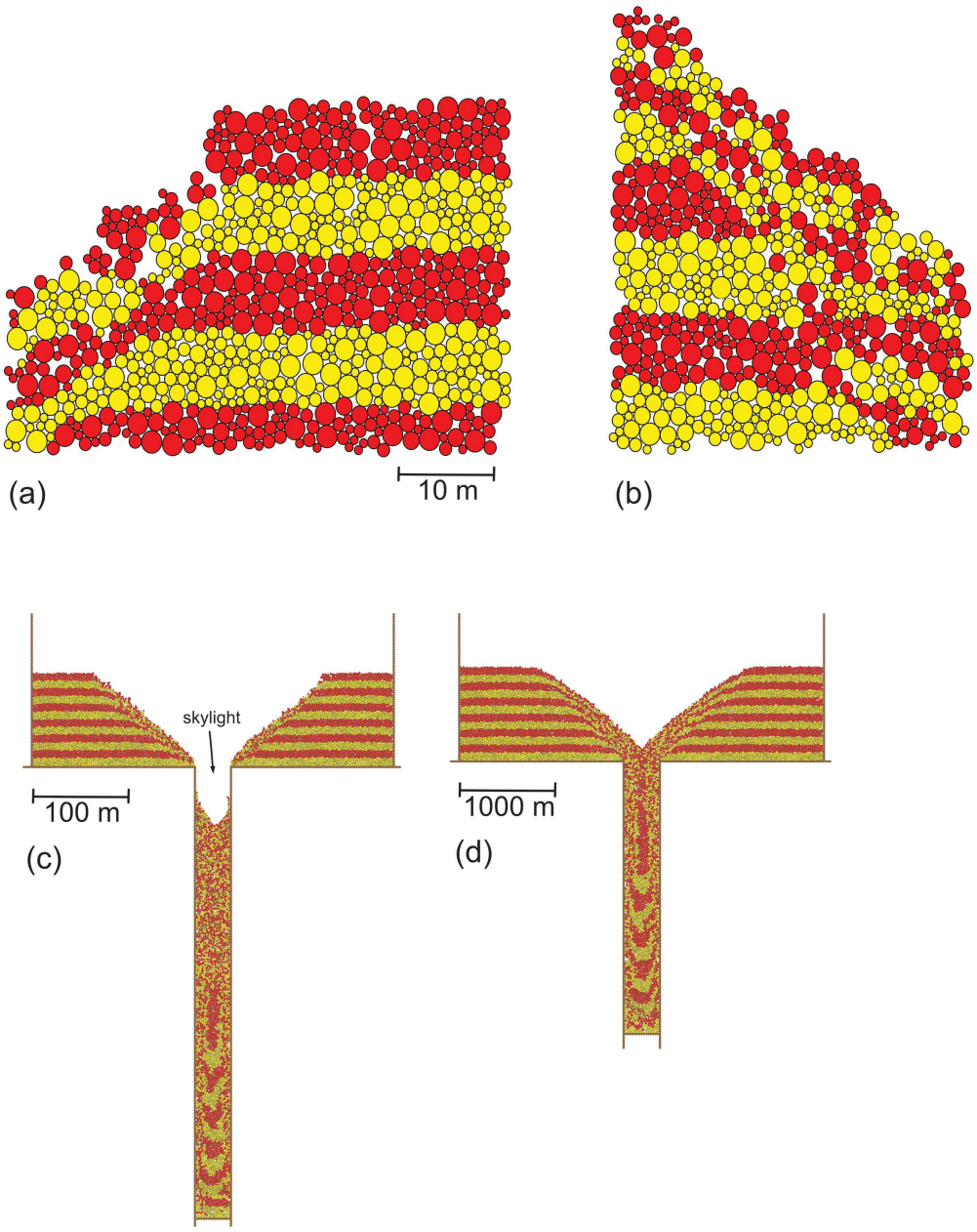


Figure 4

Figure 4. (a) Zoom of upper part of experiment shown in Fig. 3d showing distinct, steep crater rim and regolith “layering, (b) zoom of crater wall of experiment shown in Fig. 3d showing a mantle of disrupted, collapsed regolith, (c) ´skylight´ example, final static configurations after instantaneous creation of a 40 m wide void that is 500 m deep and which provides more drainage area than the frictional-cohesive regolith can fill, (d) final static configuration of a roof-collapse model with a 1000 m thick overburden, regolith is frictional. See text for discussion.

 doi:10.20944/preprints202106.0078.v1